

## Article

# A Self-Adaption Growth Model for the Burden Packing Process in a Bell-Less Blast Furnace

Dongling Wu <sup>1</sup>, Fengjie Yao <sup>1</sup>, Duoyong Zhang <sup>1</sup>, Enxue Zu <sup>1</sup>, Ping Zhou <sup>1,\*</sup> and Wei Chen <sup>2,\*</sup>

<sup>1</sup> School of Energy Science and Engineering, Central South University, Changsha 410083, China; dongling.wu@csu.edu.cn (D.W.); duoyongzhang@sjtu.edu.cn (D.Z.)

<sup>2</sup> School of Intelligent Manufacturing Ecosystem, Xi'an Jiaotong-Liverpool University, Suzhou 215123, China

\* Correspondence: zhoup@csu.edu.cn (P.Z.); wei.chen02@xjtlu.edu.cn (W.C.)

**Abstract:** The burden structure directly decides the distribution of gas flow inside a blast furnace (BF). Falling, stacking, and descending bulk materials are the three main processes for burden formation, among which the stacking process plays a decisive role. The Discrete Element Method (DEM) and theoretical modelling were combined to predict stacking behavior in this study. Falling and stacking behaviors were first simulated based on DEM. The repose angle during the stacking process and mass fraction distribution in the radial direction were analyzed. Then, the upper, centroid, and lower trajectory falling lines were determined, and a polynomial relation was found between the angle and the packing height. The influences of three parameters on the repose angle were investigated. Compared with the natural repose angle and chute inclination angle, the effects of the trajectory line depth appeared trivial. The polynomial relation between the repose angle and the packing height was specified to be a function of the natural angle of repose and the chute inclination angle. A three-trajectory falling model and quadratic expression were embedded in the theoretical model, yielding a self-adaption packing model. The model was proved reliable with a low relative error, below 15%.

**Keywords:** blast furnace; burden distribution; Discrete Element Method (DEM); flow trajectory; packing model



**Citation:** Wu, D.; Yao, F.; Zhang, D.; Zu, E.; Zhou, P.; Chen, W. A Self-Adaption Growth Model for the Burden Packing Process in a Bell-Less Blast Furnace. *Processes* **2024**, *12*, 1523. <https://doi.org/10.3390/pr12071523>

Academic Editor: Fabrizio Scala

Received: 24 May 2024

Revised: 29 June 2024

Accepted: 17 July 2024

Published: 19 July 2024



**Copyright:** © 2024 by the authors. Licensee MDPI, Basel, Switzerland. This article is an open access article distributed under the terms and conditions of the Creative Commons Attribution (CC BY) license (<https://creativecommons.org/licenses/by/4.0/>).

## 1. Introduction

The bulk material used in a blast furnace (BF) mainly includes iron ore and coke, and they are alternatively discharged from the hopper. However, the discharging modes of the two materials should be adjusted with in-furnace status, which makes the burden structure crucial to production capacity and energy consumption [1]. The formation of the burden structure inside a BF consists of five main steps in sequence [2], which are the descent of the bulk material from the discharge hopper, moving along the chute, falling from the rotating chute, stacking on the surface of the previous burden, and moving downward to form the entire burden structure, as shown in Figure 1. When bulk materials fall in the air and start to stack, their movements are sensitive to interparticle interactions, which are generally on the micro-scale and vary with particle properties. Therefore, among these five steps, the last three steps are crucial for deciding the final burden structure, and the stacking process is the core for determining the initial stock profile.

Theoretical modelling and numerical simulation are the two main methods used to obtain the entire burden structure of an industrial furnace. In theoretical modelling, the furnace is assumed to be axial symmetric [2–4]. The bulk material is simplified as a point, and its movement at each step is described by classical mechanic theory [5]. Every step of the charging process in Figure 1 can be described with a mathematical model, such as the falling, stacking [3,6], and decent models [4]. These sequential sub-models constitute one theoretical mathematical model. The burden structure of a whole furnace can therefore be described in two dimensions and obtained in a quite efficient way. As to

numerical simulation, the Discrete Element Method (DEM) has become the most widely used method because of its ability to track the movement of every charged particle. It can simulate the consistent movement of a bulk material throughout the charging process. Thus, three-dimensional and particle-scale information from the first step to the last one can be obtained.

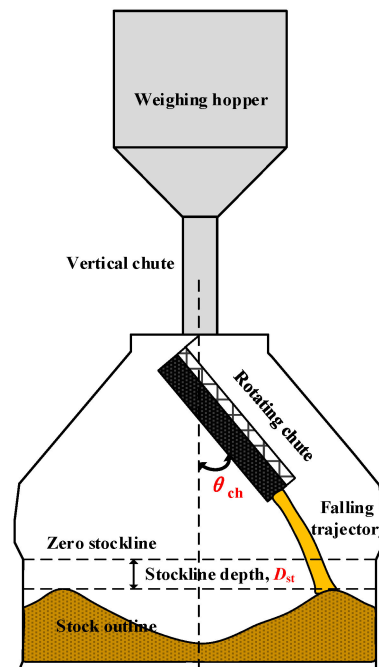


**Figure 1.** Schematic of bulk material movement and burden formation.

The formation of stock line profiles and their growth are fundamental and critical issues either in theoretical modeling and the DEM simulation method. Since the bulk material is simplified as a point in theoretical modeling, various assumptions are made in the charging process that contribute to different sub-models, including the one-trajectory-line [7] and two-line models [8,9] shown in Figure 2.

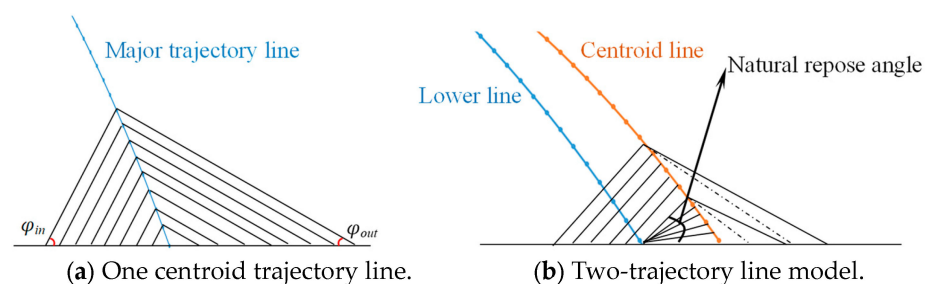


**Figure 2.** Two types of trajectory model.

In the stacking step, the falling material forms a ring-shaped heap as it reaches the previous stock surface. Different approximations can be further made to describe the stock line of the cross-section of a heap, including the piecewise linear [3,9], polynomial [10], and Gaussian approximations [11]. The linear assumption and triangular shape are used in both the one-trajectory and two-trajectory line models with the apex in the centroid trajectory. The inner and outer repose angles ( $\varphi_{in}$  and  $\varphi_{out}$ ) in the one-line trajectory falling model are then used to predict the formation of the stock line, as shown in Figure 2a. The values of  $\varphi_{in}$  and  $\varphi_{out}$  are assumed to be equal to the natural repose angle ( $\varphi_{nt}$ ). However, in previous studies, the values of the two angles have been found to be different while  $\varphi_{in}$  and  $\varphi_{nt}$  were equal [12]. In the two-line model, the outer repose angle is assumed to be equal to

$\varphi_{nt}$ . The inner repose angle is adjusted until the volume of the heap is equal to the volume of the dumped materials, as shown in Figure 2b.

The shape of the heap is a fundamental factor in the stacking process regardless of the falling trajectory model. Further studies concerning the formation of the heap therefore put emphasis on the prediction of the repose angle. Since the motion behaviors of the bulk material at the chute tip vary, the falling behaviors and subsequently formed inner and outer angles of repose are different. The inner angle is close to the center of the furnace, and, thus, it is less restricted by the furnace wall compared with the outer angle. Therefore, most earlier studies first established an inner angle prediction model and then used a similar formulation to calculate the outer angle [10,13,14]. Some of these earlier studies focused on the effects of operating parameters on the inner angle and provided valuable functions to calculate it. For example, a trigonometric function was presented by Liu [14] to describe the combined effects of the natural repose angle and the falling trajectory depth. This function was then accepted by different researchers [15–17]. The function presented by Gao et al. [13] was a linear one. It considered the effects of the falling trajectory depth and the position of the drop point. Other studies investigated the angle of repose from a particle-scale perspective. Park et al. [8,9] established a formula in which particle properties, instead of the operational parameters, were considered. These properties were the particle shape factor and particle diameter.

For the outer angle of repose, other independent functions have also been reported. The function presented by Zhu et al. [15] was a linear function in which the chute inclination angle was the only factor that affected the outer angle. Fu et al. [6,16] wrote that the outer angle was dependent on not only the chute inclination angle but also the inner angle. Since the charging parameters, such as inclination angle and trajectory line depth, are fixed for a specific furnace, the values of repose angles in theoretical mathematical models are kept constant during the charging process. In such a situation, the generated stock lines are parallel, as shown in Figure 2. This ideal growth mode of the stock line does not appear in a practical furnace as the mass distribution of the bulk material at the outlet of the chute is uneven, contributing to the uneven distribution on the previous profile in the radial direction.

For DEM simulation, both angles of repose and the stock profiles are not predefined parameters but results of the simulation. Previous studies put emphasis on the effects of particle properties and distribution patterns on these results. Wei et al. [18] investigated the relationships of the rolling friction and static friction coefficients with the repose angle and found that the coefficient of static friction behaves more sensitively to the repose angle. They further investigated the effects of the static friction coefficient on the mixture behavior of different stock profiles [19]. Other researchers have also investigated this mixture behavior by considering the effects of particle properties or shape [20–22]. Zhao et al. [23] examined the influence of the mass proportion of pellets on the whole packed bed structure of a furnace. Chen et al. [24,25] found that the deflection and width of a trajectory were sensitive to the shape of the chute. Additionally, the charged particle size varies from ~mm to ~cm, and the locations of small particles and large particles at the burden surface are different, which contributes to uneven mass distribution in the circumferential direction. This kind of size segregation requires detailed particle movement and location information, which can be easily obtained with DEM but not accessed by the theoretical charging model. Therefore, DEM is widely used to investigate size segregation phenomena during a burden charging distribution [26–29].

Since each individual iron ore and coke particle is tracked and their movement and collision behaviors are considered, there is a high demand for computational resources for DEM. To speed up the calculation, simplifications in particle size or shape are made [30,31] in the simulation. Recently, the graphics processor unit (GPU) has become an alternative computational platform for DEM, which enables the movement of tens of millions of particles and the movement of non-sphere particles to be performed within a realistic time. Combined CPU–GPU simulation has proven effective and efficient in simulating the

structure of several top layers [20,32]. However, the cost of obtaining the whole burden structure of an operating furnace remains exceptionally high. Since theoretical modelling exhibits a high calculation efficiency and DEM provides a high accuracy, the combination of the two methods seems to be a promising way to obtain a whole burden structure. Recently, a hollow cylinder test was performed in DEM simulations and automated measurement techniques have been developed to handle massive DEM simulation data to obtain the angle of repose [33,34]. These developed techniques are suitable for the purpose of creating and handling a bitmap of a heap for contact parameter calibration. However, the charging pattern of bulk material in a BF is different from the hollow cylinder test, so the extracted repose angle cannot be directly applied to a theoretical mathematical model.

In this study, the theoretical modelling method and DEM simulation were combined to develop an efficient and accurate model to describe the stacking process. Specifically, the bulk material charging process was simulated, and data regarding the formation and growth of the heap profile were analyzed. Two issues were addressed in the DEM simulations. The first one was the evaluation of the influences of the operating parameters on the angles of repose. The second one was the mathematical descriptions of the inner and outer angles of repose. Integrating the mathematical descriptions of the repose angle with the three-trajectory line, a self-adaption stacking method was developed to be used for describing the growth mode of an unparallel stock profile.

## 2. DEM Simulation of the Particle Packing Process

### 2.1. Contact Model

The Hertz–Mindlin contact model was used to describe the collision process between two particles. The contact force  $F_{ij}$  between particle  $i$  and particle  $j$  can be calculated as below.

$$F_{ij} = F_n + F_t \quad (1)$$

$$F_n = -k_n \alpha - \gamma_n v_{ij} \cdot n_{ij} \quad (2)$$

$$F_t = -k_t \delta - \gamma_t v_{ct} \quad (3)$$

where  $k$  and  $\gamma$  are the elastic and damping coefficients, respectively.  $\alpha$  means the normal overlap, and  $\delta$  refers to the tangential displacement of the contact point.  $v_{ij}$  is the relative normal velocity, while  $v_{ct}$  refers to the sliding velocity of the contact point. Therefore, as given in Equations (2) and (3), the normal force  $F_n$  consists of the elastic and damping forces, while the tangential force  $F_t$  consists of the shear and damping forces.

Friction between particles plays an important role in the stacking process. For the effects of rolling friction torque on particle motion in this study, the Elastic–Plastic Spring–Dashpot (EPSD) model developed by Ai et al. [35] was applied. The torque  $M_r$  added in EPSD is expressed in Equation (4):

$$M_r = M_r^k + M_r^d \quad (4)$$

where  $M_r^k$  and  $M_r^d$  are the elastic torque and viscous rolling torque, respectively. Equations for calculating the two torques are below:

$$\Delta M_r^k = -k_r \Delta \theta_r \quad (5)$$

where  $k_r$  is the rolling stiffness coefficient.

$$\Delta M_r^d = \begin{cases} -\eta_r C_r^{crit} \dot{\theta}_r \text{ if } |\Delta M_r^k| < M_r^m \\ -f \eta_r C_r^{crit} \dot{\theta}_r \text{ if } |\Delta M_r^k| = M_r^m \end{cases} \quad (6)$$

where  $\eta_r$  refers to the rolling viscous damping ratio.  $M_r^m$  is the limiting spring torque and is achieved at a whole mobilization rolling angle.  $\Delta \theta_r$  and  $\dot{\theta}_r$  are the incremental rotation

and relative rolling angular velocity, respectively.  $f$  is set to zero here to make the viscous damping act as a treatment to help stabilize the particles and prevent rolling oscillation.  $C_r^{crit}$  refers to the rolling critical viscous damping constant.

$$C_r^{crit} = 2\sqrt{I_r k_r} \quad (7)$$

$$I_r = 1 / \left( \frac{1}{I_i + m_i r_i^2} + \frac{1}{I_j + m_j r_j^2} \right) \quad (8)$$

where  $I_r$  is the equivalent moment of inertia for the relative rotational vibration mode about the contact point between the two contacting disks.

## 2.2. Bulk Material Flow and Stacking Process

### 2.2.1. Geometry and Parameters

The burden material flow behaviors from the chute to the stock line in a 1/15 scaled experimental furnace [36] were simulated using DEM. In this study, only the coke distribution process was considered. In this way, the simulation could be accomplished with an acceptable time cost, and the main characteristics of the stacking process could be effectively investigated. In addition, the studied geometry was 1/4 of the scaled blast furnace, as shown in Figure 3. The structural parameters of the scaled furnace are listed in Table 1. The size distribution of charged bulk material used in the scaled experiment furnace is given in Table 2. To realize the simulation, the boundary of the side surface of the 1/4 model was set as a wall but with the same properties as the particles. Additionally, the chute continuously rotated in one direction, and it started from one side in this model.

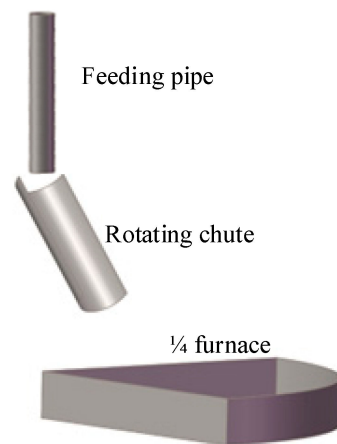


**Figure 3.** Geometry for DEM simulation.

**Table 1.** Structural parameter of the scaled furnace in DEM simulation.

Parameter	Value
Diameter of feeding pipe/mm	42
Diameter of throat/mm	553
Rotation of chute/r.min <sup>-1</sup>	8
Distance of feeding pipe/mm	650
Length of chute/mm	259.3
Chute inclination angle/degree	0–52

The properties of the coke and the collision coefficients in the contact model are given in Tables 3 and 4, respectively. The static friction and rolling stiffness coefficients were set close to that used in Ref. [37]. The natural stacking experiment determined the rolling viscous damping ratio, as shown in Figure 4.

**Table 2.** Size distribution of coke particles.

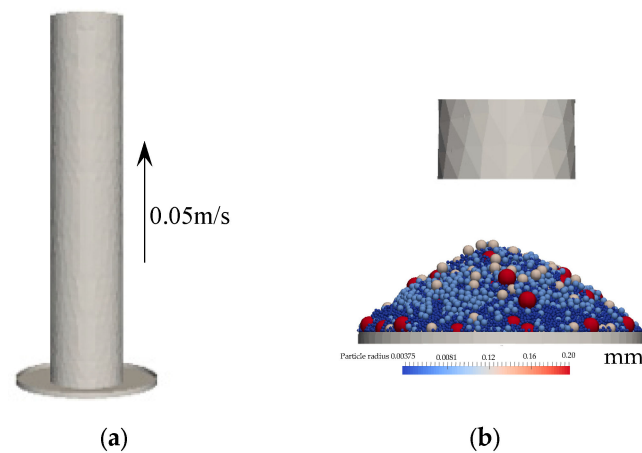
Radius ( $r/\text{mm}$ )	Percentage (wt.%)
0.6	4.0
1.125	21
1.7	46
2.325	24
2.65	5.0

**Table 3.** Particle properties.

Item	Parameters	Value
Coke	Shear modulus/MPa	5
	Poisson ratio	0.22
	Density/ $\text{kg}\cdot\text{m}^{-3}$	1000
	Natural angle of repose/ $^\circ$	34 [38]

**Table 4.** Calibrated contact coefficient.

Item	Parameters	Value
Coke–Coke	Restitution coefficient	0.18 [37]
	Static friction coefficient	0.57 [37]
	Rolling stiffness coefficient	0.35 [37]
	Rolling viscous damping ratio	0.32
Coke–Wall	Restitution coefficient	0.17 [37]
	Static friction coefficient	0.50 [37]
	Rolling stiffness coefficient	0.30 [37]
	Rolling viscous damping ratio	0.64

**Figure 4.** Simulation of the natural angle of the repose angle experiment. (a) Schematic of the natural angle of repose experiment. (b) Simulation results.

### 2.2.2. Model Validation

The model was validated with experimental data [32] in terms of trajectory lines. The parameters used in the experiment and simulation are listed in Table 5. The obtained positions of the endpoints of the upper and lower trajectory line on the horizontal plane and those obtained in the experiment are given in Table 6. The errors between the experimental and calculated data were less than 1%, proving the contact model's validity in this study.

**Table 5.** Parameters in the experiment and simulation.

Particle Diameter (d/mm)	Mass Percentage (wt.%)
<0.7	0.3
0.7 < d < 1.7	3.7
1.7 < d < 2.8	21
2.8 < d < 4	46
4 < d < 5.3	24
>5.3	5

**Table 6.** Positions of the endpoints of trajectory lines.

Distance from Endpoints to Furnace Centerline	Lower Trajectory Line	Upper Trajectory Line
Experiment data/mm	285.208	347.555
DEM results/mm	285.788	347.887

### 2.2.3. Burden Outline and Repose Angle

The outline of the generated burden surface was extracted after one circle of distribution. The extraction method and the outline after each circle are shown in Figure 5. A total number of 960 cuboid monitors were set at the cross-section of the packed burden, with 64 monitors set along the radial direction and 15 along the circumferential direction. For the  $i$ th column monitors, i.e.,  $C_i$ , all cuboid monitors in the circumferential direction ( $C_iR_1 \sim C_iR_{15}$ ) were visited to obtain the packing height and calculate the total mass of the particles in the monitor. By averaging the mass and then dividing it by the batch mass, the percentage of bulk material for the  $i$ th circle could be confirmed. By applying the traversal method to all monitors, the stock line of the cross-section of the stacking heap and mass percentage distribution in the radial direction could be obtained.

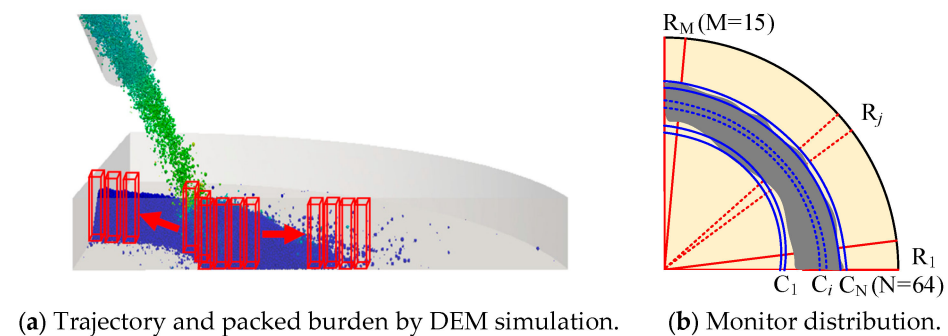
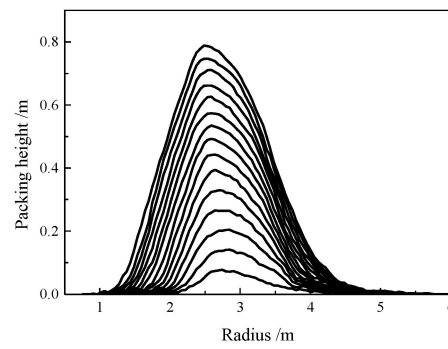
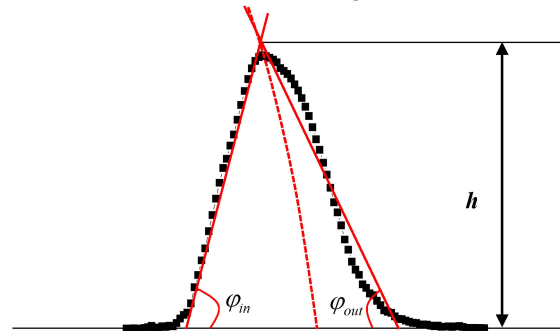
**Figure 5.** DEM simulation results and schematic of monitor setting.

Figure 6a exhibits the obtained stock lines under different circles. This indicates that the region covered by the bulk material expanded in a radial direction. Furthermore, the stock lines were not parallel, which means the repose angle could not stay unchanged as the circle increased. As previously mentioned, inner and outer repose angles are crucial parameters for predicting burden structures. Here, the inner and outer repose angles after each circle were determined with the linear fitting method with the least square method, as shown in Figure 6b. The angle between the fitted line and the horizontal plane is the inner repose angle,  $\varphi_{in}$ . By applying the linear fitting method to the right part of the outline, the outer repose angle  $\varphi_{out}$  could also be obtained.



(a) Stock lines under different distributing circles based on DEM data.



(b) Schematic of extraction of angles of repose.

**Figure 6.** Extracted stock line and repose angle from DEM data.

The inner and outer repose angles after each circle are given in Figure 7. The extracted repose angles prove that both angles gradually increased with the increased charging circles, but the outer angle changed slowly.

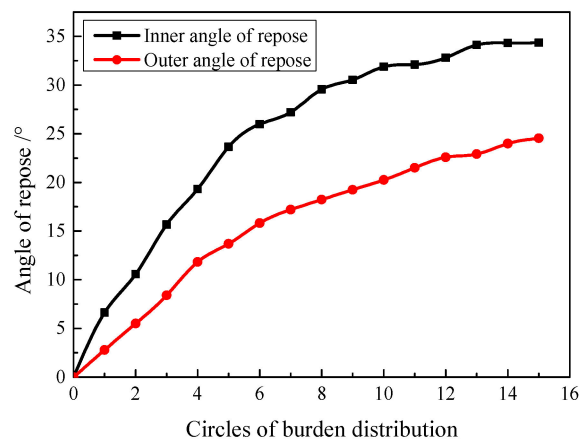


**Figure 7.** Relationship between the angle of repose and distribution circles.

The number of distributing circles is a fixed parameter set according to the furnace charging mode. Variations in the angles of repose under different circles have rarely been revealed in previous studies, making the correlation between the stacking characteristics and the angle of repose unclear. Here, by extracting the repose angle and its corresponding packing heap height, the variation tendency of the angle with the height was plotted in Figure 8. The curve in Figure 8 can be described by a quadratic function and expressed as:

$$\varphi = ah^2 + bh \quad (9)$$

where  $\varphi$  refers to the angle of repose ( $^{\circ}$ ) and  $h$  refers to the packing height (m).  $a$  and  $b$  are coefficients that relate to the charging mode and bulk material properties. The

two coefficients must be further specified if a repose-angle-predicting model needs to be established. Different simulation cases were thus set to investigate the influences of charging and property parameters on the repose angle. These influences were then quantified to obtain the values of  $a$  and  $b$ .

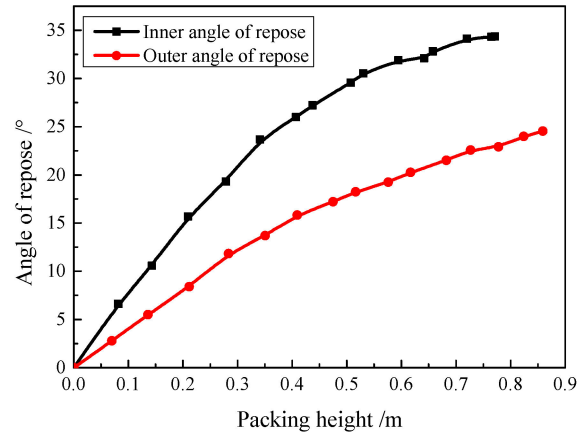


Figure 8. Variations in repose angle with the increase in packing height.

### 3. Parameter Sensitivity and Prediction Packing Model

#### 3.1. Charging and Property Parameters

Particle shape, diameter, and mechanical properties decide particle-scale contact behaviors. Consequently, these parameters considerably affect bulk materials' macro-scale dynamic flow and stacking behaviors. The natural angle of repose  $\varphi_{in}$  can characterize these macro-scale behaviors during the stacking process [35]. In addition to particle properties, the burden charging mode, especially the landing position of a bulk material, is another critical factor that can significantly change a heap profile [3,9]. The landing position is determined by those pre-steps of the stacking process, i.e., the bulk material flow in the chute and air, which is controlled by the chute inclination angle and the stock line depth. Therefore, these three parameters, namely the natural angle of repose, the chute inclination angle, and the stock line depth, are the focus of this study. The sensitivity of  $\varphi_{in}$  and  $\varphi_{out}$  to the parameters were analyzed with four investigated levels, as given in Table 7.

Table 7. Parameters investigated in this study.

Parameter	Case No.	Levels				Other Parameters
Natural angle of repose, $\varphi_0/^\circ$	NA-1~4	28.5	31.5	34.5	37.5	$\theta_{ch} = 35^\circ$ ; $D_{st} = 1.8$ m
Chute inclination $\theta_{ch}/^\circ$	CA-1~4	30	35	40	45	$\varphi_0 = 34.5^\circ$ ; $D_{st} = 1.8$ m
Stock line depth, $D_{st}/m$	SL-1~3	1.6	1.8	2.0		$\varphi_0 = 34.5^\circ$ ; $\theta_{ch} = 35^\circ$

#### 3.2. Sensitivity Analysis

Variations in the inner and outer angle of repose, along with the packing height for 15 circles, are shown in Figure 9. This suggests that both  $\varphi_{in}$  and  $\varphi_{out}$  increased as the natural angle of repose increased. A larger natural angle of repose can lead to a higher heap due to low flowability, leading to a larger repose angle. More circles were required for a small natural angle for a specific height. For instance, a packing height of 0.5 m required 11 circles with a natural repose angle of  $28.5^\circ$ , but only seven circles were enough with a natural repose angle of  $37.5^\circ$ . Compared with Figure 9a, Figure 9b exhibits slight differences in the outer angle under different values of  $\varphi_0$ .

The values of  $\varphi_{in}$  and  $\varphi_{out}$  with different packing heights when the chute inclination angle,  $\theta_{ch}$ , varied from  $30^\circ$  to  $45^\circ$  are shown in Figure 10. It is obvious that at the same packing height, a larger  $\theta_{ch}$  contributed to a larger  $\varphi_{in}$  but little change in  $\varphi_{out}$ . For a specific height, fewer circles were required for a small chute inclination angle. Correspondingly,

in a particular circle, the packing height decreased as  $\theta_{ch}$  increased. Additionally, the difference in  $\varphi_{in}$  narrowed down as the circle increased. Specifically, after distributing 15 circles, the differences in the inner angles of repose for different chute inclination angles were close to each other, but the differences in the packing height were obvious. For the outer angle of repose, with the same distribution circle, Figure 10b also shows a decrease in the packing height as  $\theta_{ch}$  increased, but the difference in  $\varphi_{out}$  was slightly larger than that in  $\varphi_{in}$ . However, it is obvious that the curves in Figure 10b exhibit the same variation tendency with packing height. This indicates that the outer profiles of the stacking heap with different chute inclination angles were parallel to each other.

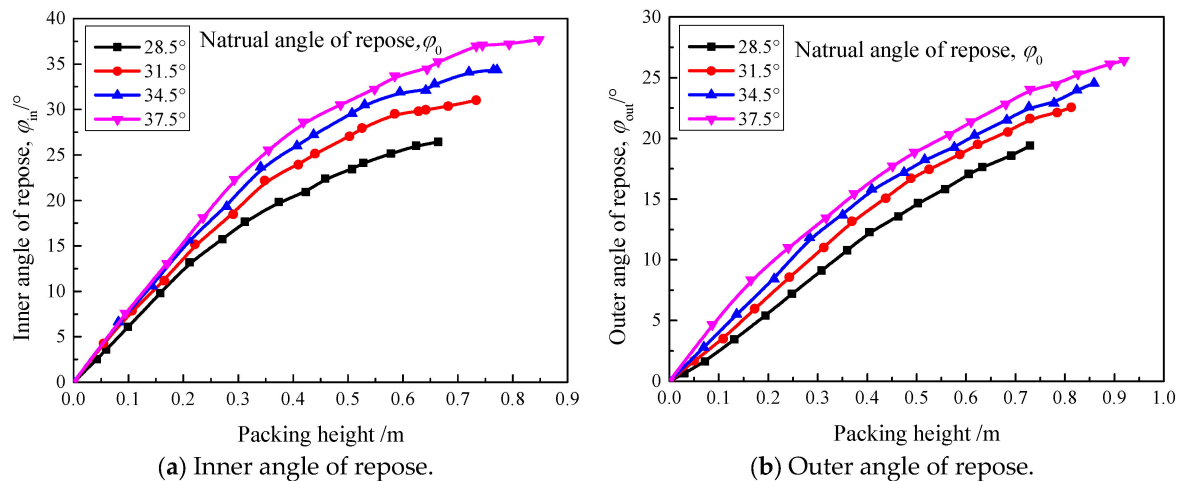


Figure 9. Variations in the angle of repose with the packing height under different natural repose angles.

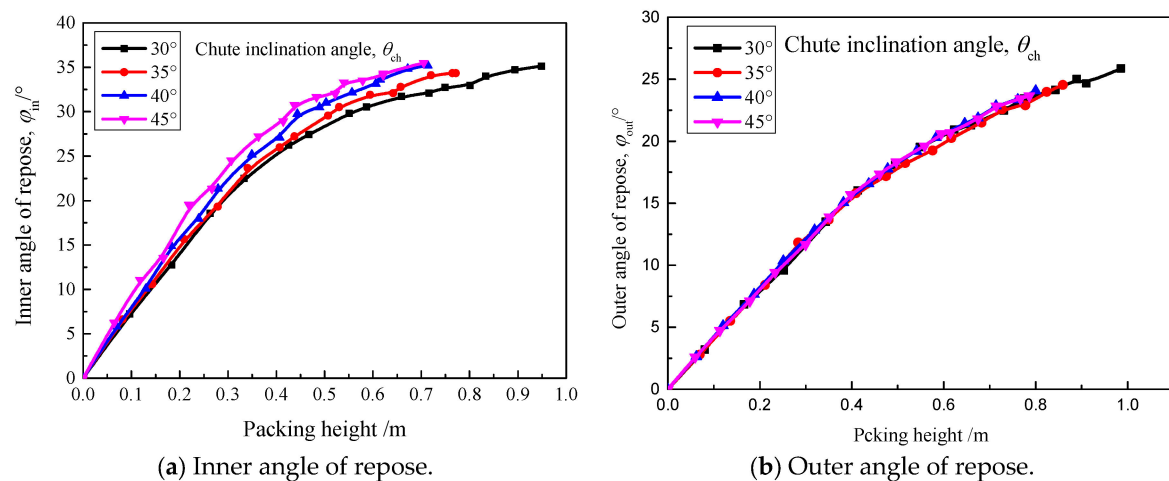
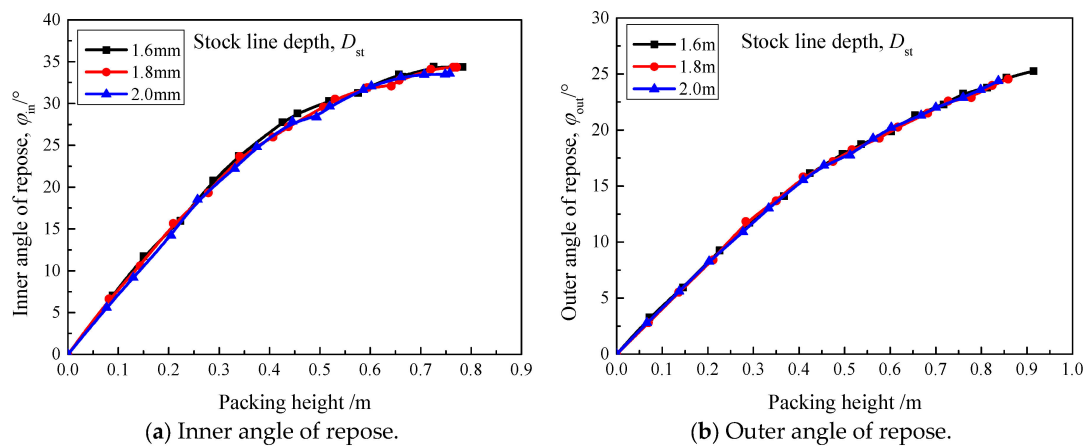


Figure 10. Variations in the angle of repose with height under different chute inclination angles.

In practical operation, the stock line depth is controlled between 1.6 m and 2.0 m. As listed in Table 6, three levels of stock line depth were investigated here. Figure 11 shows the variation in repose angles along with the packing height. It is evident that the curves either in Figure 11a or in Figure 11b exhibit the same variation tendency regardless of the stock line depth. There is a slight variation in  $\varphi_{in}$  for a specific height as the stock line depth increases, as shown in Figure 11a. However, a notable decrease in  $\varphi_{out}$  can be observed as the stock line depth increases in Figure 11b, similar to the curves in Figure 10b. The variation characteristics of the curves indicate that as the stock line depth increases, the inner profile of the heap almost remains unchanged. Still, the outer profile changes in a parallel mode.



**Figure 11.** Variations in the angle of repose with the packing height under different stock line depths.

### 3.3. Prediction Model of the Angle of Repose

As described above, the natural angle of repose and the chute inclination angle are the two parameters that considerably affect repose angles. To quantitatively describe the relationship between packing height and repose angle, the following cases in Table 8 are set as supplementary to Table 7. The calculated values of the repose angle for the cases listed in Tables 7 and 8 were fitted with Equation (9); therefore, a total number of 16 expressions of a quadratic function could be obtained. Table 9 lists the coefficients of the quadratic and linear terms of the expressions of the curves given in Figures 9 and 10. The coefficients of the other expressions for the cases in Table 8 are given in the Supplementary Materials.

**Table 8.** Supplementary cases.

Parameter	Case No.	Levels			Other Parameters
$\varphi_0/^\circ$	NA-5~7	28.5	31.5	37.5	$\theta_{ch} = 30^\circ; D_{st} = 1.8 \text{ m}$
	NA-8~10	28.5	31.5	37.5	$\theta_{ch} = 40^\circ; D_{st} = 1.8 \text{ m}$
	NA-11~13	28.5	31.5	37.5	$\theta_{ch} = 45^\circ; D_{st} = 1.8 \text{ m}$

**Table 9.** Coefficient of the fitted quadratic function.

Case No.	$a_{in}$	$b_{in}$	$R^2$	$a_{out}$	$a_{out}$	$R^2$
NA-1	−44.845	69.445	0.999	−6.433	31.756	0.998
NA-2	−50.876	76.548	0.999	−15.628	40.796	0.998
NA-3	−53.514	85.694	0.999	−21.035	46.447	0.999
NA-4	−53.075	88.967	0.997	−23.169	49.712	0.998
CA-1	−46.462	79.655	0.992	−20.364	46.042	0.994
CA-2	−53.514	85.694	0.999	−20.415	45.768	0.999
CA-3	−59.267	91.391	0.998	−21.017	46.871	0.999
CA-4	−72.655	100.630	0.997	−20.398	46.413	0.999

The coefficients of the quadratic term and the linear term above were largely decided by the sensitive charging parameters. For  $\varphi_{in}$ , the parameters were the natural angle of repose and the chute inclination angle. For  $\varphi_{out}$ , the parameter was the natural angle of repose only. By fitting the coefficients listed in Table 8 and Supplementary Materials, the following expressions describing the correlation of the coefficient with the charging parameter could be obtained.

For the inner repose angle:

$$a_{in} = 0.27\varphi_0^2 - 18.13\varphi_0 - 1.61\theta_{ch} + 310.36 \quad (R^2 = 0.956) \quad (10)$$

$$b_{in} = -0.26\varphi_0^2 + 19.45\varphi_0 + 1.23\theta_{ch} - 323.76 \quad (R^2 = 0.962) \quad (11)$$

For the outer repose angle:

$$a_{out} = 0.15\varphi_0^2 - 11.63\varphi_0 + 203.28 \quad (R^2 = 0.941) \tag{12}$$

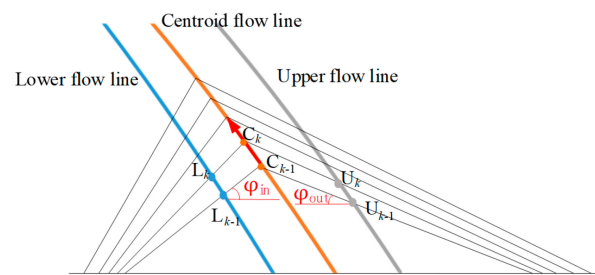
$$b_{out} = -0.12\varphi_0^2 + 9.4\varphi_0 - 143.47 \quad (R^2 = 0.958) \tag{13}$$

### 4. Stock Line Growth Method

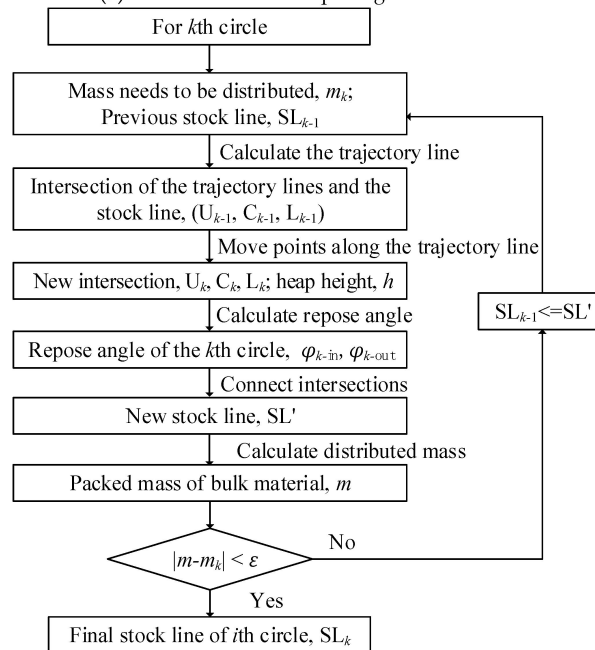
#### 4.1. Self-Adaption Growth Model

As illustrated before, the variations of the repose angle obtained with DEM in Figure 7 conflicted with the assumption in the theoretical modelling that the repose angles remain unchanged in the stacking process. To address this conflict, a self-adaption stacking and growth model was developed. The model consists of two parts. The first part is the trajectory model that considers the effects of the thickness of the trajectory. The second is the packing model with unfixed repose angles.

The three-line trajectory model used in this study consisted of the centroid, lower, and upper flow lines, as shown in Figure 12a. Two steps were used to define these flow lines. The first step was to determine the expression of the flow line, which could be confirmed according to the law of projectile motion based on the position of the endpoints on the chute and flow velocity. The second step was to confirm the endpoints of the lines. For all flow lines, one of a line's two endpoints is located at the chute outlet and the other is located on the previous stock's surface. The endpoints of the upper and lower lines on the stock surface are located where the mass percentage of bulk material is 3% in the horizontal direction. For the centroid line, the endpoint is located where the mass fraction is at the maximum value.



(a) Schematic of self-adaption growth method.



(b) Flow-chart of self-adaption growth method.

Figure 12. Procedures for determining the stock line of each circle.

The procedures for obtaining the stock line of each circle during the packing process, namely the growth of the stock line, are given in Figure 12b. The first step was to calculate the three trajectory lines, which were used to confirm the intersection points of the line with the previous stock line, as shown in Figure 12a. The intersection points were then moved upward along the trajectory line to a new position. According to the height of the new position and the expression given in Equations (10)–(13), the repose angle could be determined. The next step was to calculate the volume of the heap to evaluate whether the distributed mass had reached the set value or not. If the distributed mass was less than the set value, the new intersections continued moving along the trajectory line until the difference between the set and distributed mass was less than  $10^{-3}$ .

#### 4.2. Evaluation of the Self-Adaption Growth Model

The self-adaption growth model was evaluated using the method used in our previous study [3]. The volume enclosed by the two stock lines was calculated first. One of the lines was calculated using the theoretical modelling method, and the other was obtained using DEM, as illustrated in Figure 13. In addition to the self-adaption model, two other theoretical models, developed by Fu et al. [17] and Gao et al. [13], were evaluated. The volume was calculated as follows,

$$h_i = (|y_{D,i+1} - y_{M,i+1}| + |y_{D,i} - y_{M,i}|)/2 \quad (14)$$

$$a_i = h_i \cdot (x_{i+1} - x_i); r_i = (x_{i+1} + x_i)/2 \quad (15)$$

$$V_i = 2\pi r_i a_i \quad (16)$$

$$V_n = \sum_1^{N-1} V_i \quad (17)$$

where  $x_i$  and  $x_{i+1}$  are the horizontal distance of the  $i$ th and  $i + 1$ th point of the stock line in the radial direction.  $y_{D,i}$  and  $y_{M,i}$  are the vertical distance of the  $i$ th point of the stock line obtained with DEM and theoretical modelling, respectively.  $h_i$  and  $a_i$  denote the height and area of the quadrilateral enclosed by  $y_{D,i}$ ,  $y_{M,i}$ ,  $y_{D,i+1}$  and  $y_{M,i+1}$ .  $V_i$  refers to the volume by rotating  $a_i$  about the centerline of the furnace for one circle.  $N$  denotes the number of points set on each line; therefore,  $V_n$  refers to the total volume enclosed by the two stock lines.

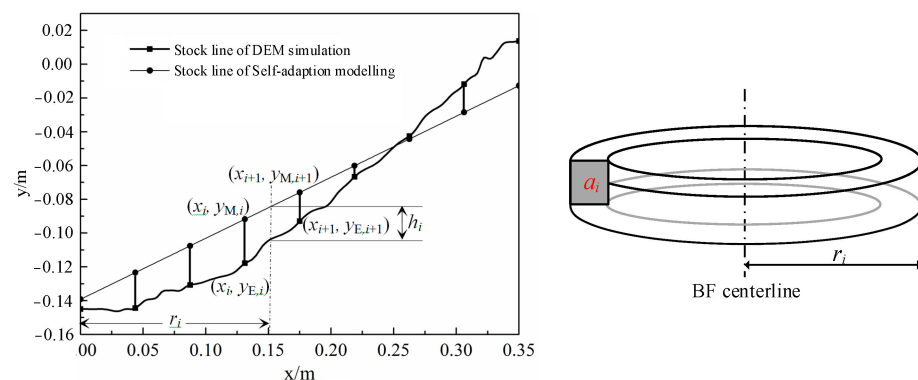


**Figure 13.** Schematic of relative error calculation.

The ratio of the enclosed volume to the distributed volume of the current circle was then calculated. Obviously, a small ratio represents high precision. The volume ratio, namely the relative error between the DEM and the theoretical modelling data, is defined as follows.

$$Er = \frac{V_n}{V} \quad (18)$$

The errors between the results obtained by the different theoretical models and validated DEM data are shown in Figure 14. For different bulk material distributing circles, the errors between the self-adaption modelling results and DEM data were less than 15% and

smaller than the errors between the other theoretical modelling results and DEM data. The self-adaption packing model was then validated.

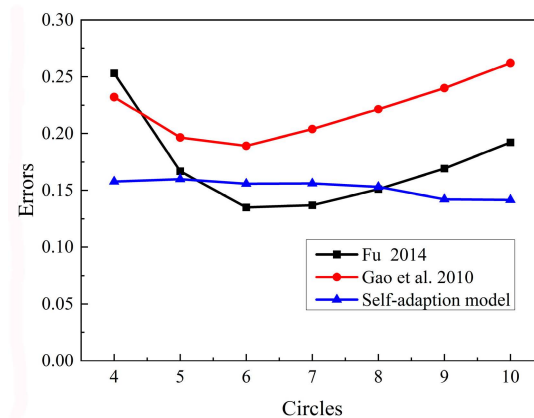


**Figure 14.** Errors between the results from Fu’s model [17] and Gao’s model [13] and DEM simulation.

## 5. Conclusions

The burden packing process was simulated with DEM. The outline of the burden surface was obtained, and the angles of repose were extracted. A new packing model was proposed to analyze the influences of three key parameters on the packing process. The main conclusions are given below.

- (1) The inner and outer angles of repose vary during the packing process and cannot remain unchanged at different distributing circles.
- (2) Compared with the chute inclination angle and stock line depth, the natural angle of repose plays an obvious role in the packing process. At the same distribution circle, the packing height decreases as the chute inclination angle increases, but it increases as the natural angle of repose increases and almost remains the same as the stock line depth increases.
- (3) Correlations between distributing parameters and repose angles were established with quadratic expressions. Combined with the correlation and centroid, upper, and lower trajectory lines, a self-adaption model was proposed with a relative error below 15%.

**Supplementary Materials:** The following supporting information can be downloaded at: <https://www.mdpi.com/article/10.3390/pr12071523/s1>, Table S1: Coefficient of the fitted quadratic of 16 cases; Table S2: Contact parameters needed to be calibrated; Table S3: Levels of each parameters; Table S4 DEM simulation results of each cases; Table S5: Possible values of contact parameters; Table S6: Calibrated values of contact parameters.

**Author Contributions:** Conceptualization, D.W. and E.Z.; methodology, W.C., D.Z. and E.Z.; software, D.Z. and E.Z.; validation, F.Y. and D.W.; formal analysis, E.Z. and D.W.; investigation, F.Y.; resources, E.Z. and D.Z.; data curation, E.Z. and D.W.; writing—original draft preparation, D.Z. and D.W.; writing—review and editing, D.W. and F.Y.; visualization, E.Z.; supervision, P.Z.; project administration, D.W. and P.Z.; funding acquisition, D.W. All authors have read and agreed to the published version of the manuscript.

**Funding:** This work was supported by the National Natural Science Foundation of China (No. 52106217) and the Natural Science Foundation of Hunan Province (Grant No. 2021JJ40763).

**Data Availability Statement:** The data presented in this study are available in Supplementary Materials.

**Conflicts of Interest:** The authors declare no conflict of interest.

## References

1. Bambauer, F.; Wirtz, S.; Scherer, V.; Bartusch, H. Transient dem-cfd simulation of solid and fluid flow in a three dimensional blast furnace model. *Powder Technol.* **2018**, *334*, 53–64. [\[CrossRef\]](#)
2. Zhou, C. *Minimization of Blast Furnace Fuel Rate by Optimizing Burden and Gas Distribution*; University Libraries: Washington, DC, USA, 2012.
3. Shi, P.Y.; Fu, D.; Zhou, P.; Zhou, C.Q. Evaluation of stock profile models for burden distribution in blast furnace. *Ironmak. Steelmak.* **2015**, *42*, 756–762. [\[CrossRef\]](#)
4. Zhou, P.; Shi, P.-Y.; Song, Y.-P.; Tang, K.-L.; Fu, D.; Zhou, C.Q. Evaluation of burden descent model for burden distribution in blast furnace. *J. Iron Steel Res. Int.* **2016**, *23*, 765–771. [\[CrossRef\]](#)
5. Shi, P.Y.; Zhou, P.; Fu, D.; Zhou, C.Q. Mathematical model for burden distribution in blast furnace. *Ironmak. Steelmak.* **2016**, *43*, 74–81. [\[CrossRef\]](#)
6. Fu, D.; Chen, Y.; Zhou, C.Q. Mathematical modeling of blast furnace burden distribution with non-uniform descending speed. *Appl. Math. Model.* **2015**, *39*, 7554–7567. [\[CrossRef\]](#)
7. Radhakrishnan, V.R.; Maruthy Ram, K. Mathematical model for predictive control of the bell-less top charging system of a blast furnace. *J. Process Control* **2001**, *11*, 565–586. [\[CrossRef\]](#)
8. Park, J.I.; Baek, U.H.; Jang, K.S.; Oh, H.S.; Han, J.W. Development of the burden distribution and gas flow model in the blast furnace shaft. *Trans. Iron Steel Inst. Jpn.* **2011**, *51*, 1617–1623. [\[CrossRef\]](#)
9. Park, J.I.; Jung, H.J.; Jo, M.K.; Oh, H.S.; Han, J.W. Mathematical modeling of the burden distribution in the blast furnace shaft. *Met. Mater. Int.* **2011**, *17*, 485–496. [\[CrossRef\]](#)
10. Hattori, M.; Iino, B.; Shimomura, A.; Tsukiji, H.; Ariyama, T. Development of burden distribution simulation model for bell-less top in a large blast furnace and its application. *ISIJ Int.* **1993**, *33*, 1070–1077. [\[CrossRef\]](#)
11. Nag, S.; Gupta, A.; Paul, S.; Gavel, D.J.; Aich, B. Prediction of heap shape in blast furnace burden distribution. *ISIJ Int.* **2014**, *54*, 1517–1520. [\[CrossRef\]](#)
12. Chen, J.S.; Zuo, H.B.; Wang, J.X.; Xue, Q.G.; Wang, J.S. Mathematical model of burden distribution in bell-less top blast furnace. *J. Iron Steel Res. Int.* **2023**, *30*, 216–226. [\[CrossRef\]](#)
13. Gao, X.D.; Cheng, S.S.; Du, P.Y. Mathematical model of the burden surface for bell-less blast furnace top. *Metall. Autom.* **2009**, *S1*, 652–655.
14. Liu, Y.C. *Charging Rules of Blast Furnace*, 2nd ed.; Metallurgical Industry Press: Beijing, China, 2005.
15. Zhu, Q.; Lü, C.L.; Yin, Y.X.; Chen, X.Z. Burden distribution calculation of bell-less top of blast furnace based on multi-radar data. *J. Iron Steel Res. Int.* **2013**, *20*, 33–37. [\[CrossRef\]](#)
16. Fu, D.; Huang, F.; Tian, F.; Zhou, C. Burden descending and redistribution in a blast furnace. In Proceedings of the Association for Iron & Steel Technology Conference 2010, Pittsburgh, PA, USA, 3–6 May 2010; AISTech: Pittsburgh, PA, USA, 2010.
17. Fu, D. Numerical Simulation of Ironmaking Blast Furnace Shaft, Dissertations & Theses Gradworks. Ph.D. Thesis, Purdue University, West Lafayette, IN, USA, 2014.
18. Wei, S.; Wei, H.; Saxen, H.; Yu, Y. Numerical analysis of the relationship between friction coefficient and repose angle of blast furnace raw materials by discrete element method. *Materials* **2022**, *15*, 903. [\[CrossRef\]](#) [\[PubMed\]](#)
19. Wei, H.; Saxen, H.; Yu, Y. Numerical analysis of factors affecting the burden surface and porosity distribution in the upper part of the blast furnace. *Metals* **2023**, *13*, 292. [\[CrossRef\]](#)
20. Govender, N.; Wilke, D.N.; Wu, C.-Y.; Tuzun, U.; Kureck, H. A numerical investigation into the effect of angular particle shape on blast furnace burden topography and percolation using a gpu solved discrete element model. *Chem. Eng. Sci.* **2019**, *204*, 9–26. [\[CrossRef\]](#)
21. Yu, Y.; Saxén, H. Effect of dem parameters on the simulated inter-particle percolation of pellets into coke during burden descent in the blast furnace. *ISIJ Int.* **2012**, *52*, 788–796. [\[CrossRef\]](#)
22. Khanal, M.; Elmoultie, M.; Adhikary, D. Effects of particle shapes to achieve angle of repose and force displacement behaviour on granular assembly. *Adv. Powder Technol.* **2017**, *28*, 1972–1976. [\[CrossRef\]](#)
23. Zhao, Z.J.; Saxen, H.; Liu, Y.J.; She, X.F.; Xue, Q.G. Numerical study on the influence of pellet proportion on burden distribution in blast furnace. *Ironmak. Steelmak.* **2022**, *50*, 613–620. [\[CrossRef\]](#)
24. Chen, J.S.; Zuo, H.B.; Wang, Y.J.; Xue, Q.G.; Wang, J.S. Dem simulation of burden circumferential distribution of blast furnace with parallel hoppers. *Metall. Mater. Trans. B Process Metall. Mater. Process. Sci.* **2022**, *53*, 3793–3804. [\[CrossRef\]](#)
25. Chen, J.S.; Zuo, H.B.; Zhao, H.B.; Xue, Q.G.; Wang, J.S. Burden circumferential mass segregation at the blast furnace with parallel hoppers. *Powder Technol.* **2022**, *409*, 117845. [\[CrossRef\]](#)
26. Hiroshi, M.; Yoichi, N.; Kaoru, N.; Seiji, N. Validation of the Burden Distribution of the 1/3-Scale of a Blast Furnace Simulated by the Discrete Element Method. *Processes* **2019**, *8*, 6. [\[CrossRef\]](#)
27. Xu, W.; Cheng, S.; Niu, Q.; Hu, W.; Bang, J. The DEM study of segregation phenomena of burden distribution during the charging process of blast furnace with two parallel hoppers. *Ironmak. Steelmak.* **2020**, *47*, 337–343. [\[CrossRef\]](#)
28. Zhang, T.F.; Gan, J.Q.; Yu, A.B.; Pinson, D.; Zhou, Z.Y. Size segregation of granular materials during Paul-Wurth hopper charging and discharging process. *Powder Technol.* **2020**, *378*, 497–509. [\[CrossRef\]](#)
29. Li, C.X.; Dong, K.J.; Liu, S.D. DEM study of particle segregation in the throat region of a blast furnace. *Powder Technol.* **2022**, *407*, 117660. [\[CrossRef\]](#)

30. Ueda, S.; Natsui, S.; Fan, Z.; Nogami, H.; Soda, R.; Kano, J.; Inoue, R.; Ariyama, T. Influences of physical properties of particle in discrete element method on descending phenomena and stress distribution in blast furnace. *ISIJ Int.* **2010**, *50*, 981–986. [[CrossRef](#)]
31. Ariyama, T.; Natsui, S.; Kon, T.; Ueda, S.; Kikuchi, S.; Nogami, H. Recent progress on advanced blast furnace mathematical models based on discrete method. *ISIJ Int.* **2014**, *54*, 1457. [[CrossRef](#)]
32. Govender, N.; Wilke, D.N.; Kok, S. Collision detection of convex polyhedra on the nvidia gpu architecture for the discrete element method. *Appl. Math. Comput.* **2015**, *267*, 810–829. [[CrossRef](#)]
33. Muller, D.; Fimbinger, E.; Brand, C. Algorithm for the determination of the angle of repose in bulk material analysis. *Powder Technol.* **2021**, *383*, 598–605. [[CrossRef](#)]
34. Tan, Y.; Yu, Y.; Fottner, J.; Kessler, S. Automated measurement of the numerical angle of repose of biomass particles in edem with a novel algorithm. *Powder Technol.* **2021**, *388*, 462–473. [[CrossRef](#)]
35. Ai, J.; Chen, J.F.; Rotter, J.M.; Jin, Y.O. Assessment of rolling resistance models in discrete element simulations. *Powder Technol.* **2011**, *206*, 269–282. [[CrossRef](#)]
36. Liang, D.; Yu, Y.W.; Bai, C.G.; Qiu, G.B.; Zhang, S.F. Effect of burden material size on blast furnace stockline profile of bell-less blast furnace. *Ironmak. Steelmak.* **2009**, *36*, 217–221. [[CrossRef](#)]
37. Xu, W.; Cheng, S.; Niu, Q.; Zhao, G. Effect of the main feeding belt position on burden distribution during the charging process of bell-less top blast furnace with two parallel hoppers. *ISIJ Int.* **2017**, *57*, 1173–1180.
38. Jimenez, J.; Mochón, J.; Formoso, A.; de Ayala, J.S. Burden distribution analysis by digital image processing in a scale model of a blast furnace shaft. *ISIJ Int.* **2000**, *40*, 114–120. [[CrossRef](#)]

**Disclaimer/Publisher’s Note:** The statements, opinions and data contained in all publications are solely those of the individual author(s) and contributor(s) and not of MDPI and/or the editor(s). MDPI and/or the editor(s) disclaim responsibility for any injury to people or property resulting from any ideas, methods, instructions or products referred to in the content.